Gut microbiota density influences host physiology and is shaped by host and microbial factors

Eduardo J. Contijoch[1,2], Graham J. Britton[1,2], Chao Yang[1,2], Ilaria Mogno[1,2], Zhihua Li[1,2], Ruby Ng[1,2], Sean R. Llewellyn[1,2], Sheela Hira[3], Crystal Johnson[4], Keren M. Rabinowitz[5,6], Revital Barkan[5], Iris Dotan[5,7], Robert P. Hirten[8], Shih-Chen Fu[2], Yuying Luo[8], Nancy Yang[8], Tramy Luong[2], Philippe R. Labrias[2], Sergio A. Lira[1], Inga Peter[2], Ari Grinspan[8], Jose C. Clemente[1,2], Roman Kosoy[2], Seunghee Kim-Schulze[9], Xiaochen Qin[1], Anabella Castillo[8], Amanda Hurley[2], Ashish Atreja[8], Jason Rogers[8], Farah Fasihuddin[8], Merjona Saliaj[8], Amy Nolan[8], Pamela Reyes-Mercedes[8], Carina Rodriguez[8], Sarah Aly[8], Kenneth Santa-Cruz[8], Lauren A. Peters[2,10,11], Mayte Suárez-Fariñas[2], Ruiqi Huang[2], Ke Hao[2], Jun Zhu[2], Bin Zhang[2], Bojan Losic[2], Haritz Irizar[2], Won-Min Song[2], Antonio Di Narzo[2], Wenhui Wang[2], Benjamin L. Cohen[8], Christopher DiMaio[8], David Greenwald[8], Steven Itzkowitz[8], Aimee Lucas[8], James Marion[8], Elana Maser[8], Ryan Ungaro[8], Steven Naymagon[8], Joshua Novak[8], Brijen Shah[8], Thomas Ullman[8], Peter Rubin[8], James George[8], Peter Legnani[8], Shannon E Telesco[12], Joshua R. Friedman[12], Carrie Brodmerkel[12], Scott Plevy[12], Judy Cho[8], Jean-Frederic Colombel[8], Eric Schadt[2,11], Carmen Argmann[2], Marla Dubinsky[13], Andrew Kasarskis[2], Bruce Sands[8], Jeremiah J. Faith[1,2,14*]

1. Precision Immunology Institute, Icahn School of Medicine at Mount Sinai, New York, NY, 10029, USA
2. Icahn Institute for Genomics and Multiscale Biology, Icahn School of Medicine at Mount Sinai, New York, NY, 10029, USA
3. Zoo Knoxville, Knoxville, TN, 37914, USA
4. Center for Comparative Medicine and Surgery, Icahn School of Medicine at Mount Sinai, New York, NY, 10029, USA
5. Division of Gastroenterology, Rabin Medical Center, Beilinson Campus, Petah Tikva, 4941492, Israel
6. Felsenstein Medical Research Center, Sackler Faculty of Medicine, Tel Aviv University, Tel Aviv 6997801 Israel
7. Sackler Faculty of Medicine, Tel Aviv University, Tel Aviv 6997801, Israel
8. The Dr. Henry D. Janowitz Division of Gastroenterology, Icahn School of Medicine at Mount Sinai, New York, NY, 10029, USA
9. Division of Hematology and Medical Oncology, The Tisch Cancer Institute, Icahn School of Medicine at Mount Sinai, New York, NY, 10029, USA
10. Department of Genetics & Genomic Sciences, Icahn School of Medicine at Mount Sinai, New York, NY, 10029, USA
11. Sema4, a Mount Sinai venture, Stamford, CT, 06902, USA
12. Janssen Research and Development, LLC., Spring House, Pennsylvania, 19002, USA
13. Pediatric Gastroenterology and Hepatology, Department of Pediatrics, Susan and Leonard Feinstein IBD Clinical Center, Icahn School of Medicine at Mount Sinai, New York, NY, 10029, USA
14. Lead Contact

*Correspondence: jeremiah.faith@mssm.edu

Summary

To identify factors that regulate the absolute microbiota and the impact of varied microbiota density on health, we assayed gut microbiota density across mammals, disease, and therapeutic interventions. Physiologic features of the host (carrying capacity) and the fitness of the gut microbiota shape microbiota density. Therapeutic manipulation of microbiota density in mice altered host metabolic and immune homeostasis. In humans, gut microbiota density was reduced in Crohn's disease, ulcerative colitis, and ileal pouch-anal anastomosis. The gut microbiota in recurrent *Clostridium difficile* infection had lower density and reduced fitness that were restored by fecal microbiota transplantation. Understanding the interplay between microbiota and disease through the conceptual framework of microbiota density, host carrying capacity, and microbiota fitness could provide biomarkers to identify candidates for microbiota therapeutics and monitor their response.

Introduction

The relationships uncovered between the gut microbiota and health have largely focused on relative community differences, estimated with culture-independent 16S rDNA (Caporaso et al., 2010; Schloss et al., 2009) or shotgun metagenomic sequencing (Segata et al., 2012), and do not resolve changes in the absolute abundance of a given taxa. We hypothesized that the microbiome's influence on host physiology depends on the number – and not just the type – of bacteria interfacing with the host. Therefore, understanding factors driving gut microbiota density, as well as the impact of microbiota density and absolute changes in microbial taxa on health may advance the therapeutic potential of the microbiota. These absolute changes can be determined by combining compositional methods with an estimate of the microbial community size (microbiota density). Microbiota density has previously been measured with colony-forming units, sequencing spike-ins (Satinsky et al., 2013; Stämmler et al., 2016), qPCR (Mahowald et al., 2009; Rey et al., 2013), flow cytometry (Props et al., 2017; Reyes et al., 2013; Vandeputte et al., 2017), and microbial DNA quantification (microbial DNA per mass of sample) (Faith et al., 2011; Llewellyn et al., 2017; Reyes et al., 2013). Here, we use microbial DNA content to estimate community size, since it correlates with bacterial cell counts and can be incorporated into standard microbiome sequencing workflows by simply weighing the sample (Reyes et al., 2013). We investigate host and microbial factors that contribute to microbiota density, study the impact of microbiota density on host physiology, and describe absolute alterations of the microbiome in disease and the resolution of those alterations after therapy in ways that are not captured by compositional methods alone.

Results

The natural variation of gut microbiota density in mammals is driven by host and microbial factors

In macroecology, carrying capacity is the maximal density of organisms supported by an ecosystem and is broadly dictated by the resources (*e.g.* food, water, and habitat) in the environment. Whether or not the collection of species in an environment can reach the carrying capacity depends on their ability to efficiently utilize the resources available (fitness). To explore these concepts and their contribution to microbiota density, we collected fecal material from sixteen different mammals (Table S1) in order to sample a diverse range different host intestinal architectures and gut microbial community compositions. Using methods optimized to assay fecal microbiota density with greater throughput (see Methods and Figure S1), we observed significant differences in microbiota density across our mammalian samples ($F = 11.06$, $p = 7.66 \times 10^{-15}$; ANOVA) with a 53-fold difference between the most dense and least dense gut microbiota (Figure 1A). We found a positive correlation between microbiota density and phylogenetic relatedness of the host ($r = 0.222$; $p = 0.0150$; Pearson; Figure 1B), while there was no correlation between fecal water content and microbiota density ($\rho = -0.130$, $p = 0.660$, Spearman; Figure 1C). Animals from order *Carnivora* (dog, ferret, lion, red panda, and tiger), with simple gut architectures adapted to carnivorous diets, had significantly reduced microbiota densities compared with the rest of the mammals studied ($p = 3.26 \times 10^{-16}$, Welch's t-test; Figure 1D).

To study the contribution of host carrying capacity and microbiota fitness to microbiota density, we utilized gnotobiotic mice with controlled host carrying capacity (*i.e* fixed diet, genetics, and environment) colonized with different microbiotas. In germ-free Swiss Webster mice colonized with four of the lowest density microbiotas in our initial screen (lion, elephant, ferret, and red panda), the lion and red panda microbiotas reached higher microbiota densities in the mouse than in the native host,

suggesting their densities were limited by the carrying capacity of their host. The elephant and ferret microbiotas colonized mice at densities comparable to those in the native host and significantly less dense than a mouse microbiota (Figure 1E). These results demonstrate that as in macroecology, microbiota density represents the combined influence of host carrying capacity and microbiota fitness.

Absolute microbial dynamics in response to pharmacologics

Culture-independent measurements have revealed that antibiotics can disrupt the composition of a healthy gut microbiota (Dethlefsen et al., 2008). We hypothesized that antibiotics may also have an impact on the gut microbiota density. To test this hypothesis, we administered vancomycin in two doses (0.2 mg/mL and 0.5 mg/mL) to two sets of SPF C57BL/6J mice and collected fecal pellets before and during treatment. We found that vancomycin exerted selective pressure against susceptible organisms leading to a relative expansion of Verrucomicrobia and Firmicutes in the low and high dose groups respectively (Figures 2A and 2B). When we multiplied each taxa's relative abundance by the microbiota density to calculate their absolute abundances, we observed a bloom of Verrucomicrobia in the low dose group (Figure 2C). Surprisingly, in the high dose group, we found that vancomycin successfully depleted members of all phyla, including Firmicutes (Figure 2D). Microbiota density and alpha diversity were not significantly correlated (ρ = 0.107; p = 0.557; Spearman; Figure S2A), as both low dose and high dose vancomycin significantly reduced alpha diversity (p_{low} = 1.56 x 10^{-7} and p_{high} = 0.0161, vs baseline, Dunnett's test; Figure S2B), while only high dose vancomycin reduced microbiota density (p_{low} = 0.910, p_{high} = 8.61 x 10^{-7}, vs baseline, Dunnett's test; Figure S2C).

To more broadly assess the impact of therapeutics on the absolute gut microbiota, we provided SPF mice with one of 20 orally administered drugs, including antibiotics, anti-motility agents, and laxatives (Table S2). Only 9 of the 14 tested antibiotics significantly decreased gut microbiota density compared to untreated animals ($p < 0.05$ for each; Dunnett's test). Amongst these 9 density-reducing antibiotics, there were substantial differences in each drug's depleting capacity (Figure 2E). Of the laxatives, PEG 3350 reduced microbiota density (p = 3.03 x 10^{-5}), while lactulose increased it (p = 8.57 x 10^{-5}). The anti-motility agent loperamide increased microbiota density (p = 1.86 x 10^{-4}), while the proton pump inhibitor omeprazole had no effect. To test the resilience of two healthy human microbiotas (Hu_001 and Hu_002) to antibiotics, we depleted the density of gnotobiotic Swiss Webster mice colonized with each donor using a cocktail of ampicillin, vancomycin (high dose), neomycin, and clindamycin (p = 2.87 x 10^{-4} for Hu_001; p = 1.63 x 10^{-4} for Hu_002, Tukey's HSD; Figure 2F). The Hu_001 antibiotic-treated microbiota transferred to new gnotobiotic mice without antibiotics had reduced microbiota density (p = 0.0497, Tukey's HSD; Figure 2F), demonstrating antibiotics can permanently alter the gut microbiota to reduce fitness (Blaser, 2014; Dethlefsen and Relman, 2011).

Manipulation of colonic microbiota density alters host physiology

Comparing antibiotic-treated or germ-free mice with conventional mice has demonstrated the influence of the microbiota on a range of physiological measures (Atarashi et al., 2011; Bäckhed et al., 2004; Bongers et al., 2014; Faith et al., 2014; Geuking et al., 2011; Ivanov et al., 2009; Mortha et al., 2014; Muller et al., 2014; Ridaura et al., 2013; Wostmann B and Bruckner-Kardoss, 1959; Zhang et al., 2015). To better understand the impact of microbiota density on host physiology, we selected five antibiotics (ampicillin, ciprofloxacin, clindamycin, polymyxin B, vancomycin) based on their varying ability to decrease microbiota density (Figure 2E). As expected, treating 4-week old SPF C57BL/6J mice with each antibiotic in their drinking water (n = 6 mice per antibiotic, 9 SPF antibiotic-free controls, and 6 germ-free controls) led to a range of density

reductions across the experimental groups (1.2 – 56.6 fold; Figure S3A). We found a significant negative correlation between cecum size and microbiota density (ρ = -0.729, p = 2.46 x 10^{-7}, Spearman; Figures 3A and S3B). Epididymal fat pad mass, fecal IgA, and lamina propria FoxP3+CD4+ regulatory T cells were each positively correlated with microbiota density (ρ_{fat} = 0.587, p_{fat} = 6.11 x 10^{-5}; ρ_{IgA} = 0.783, p_{IgA} = 3.35 x 10^{-7}; ρ_{Treg} = 0.639, p_{Treg} = 5.31 x 10^{-6}; Spearman; Figures 3B-3D and S3C-S3E).

To further understand the impact of antibiotic treatment and microbiota density on host physiology, we measured changes in transcript-level gene expression by RNA sequencing of proximal colon tissue from a subset of these mice (n = 3 for each antibiotic; n = 4 for the germ-free group; n = 5 for the control group). Microbiota density was correlated with the expression of 89 transcripts (FDR < 0.05, Table S3). Hierarchical clustering by the expression of these transcripts grouped together samples from germ-free animals and those given antibiotics that reduce microbiota density the greatest (ampicillin, clindamycin, and vancomycin; Figure 3E). The genes *Ensa*, *Fam192a*, and *Gde1* were the most correlated with microbiota density (ρ_{Ensa} = -0.865, $\rho_{Fam192a}$ = 0.853, ρ_{Gde1} = -0.851, p < 10^{-16}; Spearman; Figures 3F-3H). Together, these results suggest that gut microbiota density influences the metabolic, immunological, and transcriptional profiles of the host.

The absolute microbiome of inflammatory bowel disease (IBD)

To characterize the gut microbiota of subjects with IBD in absolute terms, we collected fecal samples from 70 healthy controls, 144 subjects with Crohn's disease (CD), 109 subjects with ulcerative colitis (UC), and 19 subjects with UC that had undergone an ileal pouch-anal anastomosis (IPAA) procedure following total colectomy. Concordant with prior work using phylum-specific qPCR (Frank et al., 2007) and flow cytometry (CD-only; Vandeputte et al., 2017), subjects with IBD had decreased microbiota density compared to healthy controls (p < 0.001 for each vs Healthy, Tukey's HSD; Figure 4A), even when excluding individuals receiving antibiotics (Figure S4A). Individuals with active CD or UC, as well as IPAA subjects had increased fecal water content compared to healthy individuals (p < 0.05 for each vs Healthy; Tukey's HSD), while individuals with inactive CD or UC did not. Nonetheless, the decrease in microbiota density in IBD compared to healthy controls was consistent across individuals with active disease or inactive disease (p < 0.001 for each vs Healthy, Tukey's HSD; Figure 4B), suggesting the microbiota density changes in IBD were not simply driven by active inflammation. We performed gnotobiotic transfer experiments which demonstrated that the IPAA microbiota had reduced community fitness (Figure S4B) that may result from the inability of high density colonic microbes to efficiently colonize the unique gut architecture of individuals with IPAA.

In line with previous studies (Frank et al., 2007; Gevers et al., 2014; Gophna et al., 2006; Jacobs et al., 2016), the IBD microbiome had a decreased alpha diversity compared to healthy subjects (p < 0.01 for all; Tukey's HSD; Figure S4C) and a relative increase in Proteobacteria (p < 0.01 for CD and IPAA vs Healthy, Dunnett's test; Figure 4C). Remarkably, in absolute terms Proteobacteria do not increase in UC or CD (Figure 4D). We hypothesized that Proteobacteria are uniquely capable of maintaining a given density independent of the other major phyla in the gut microbiota. Proteobacteria were the only phyla among the four major phyla of the gut microbiota that were not correlated with microbiota density (Figures 4E-4H). These results indicate that the differences in IBD microbiome may be driven by differences in the abundance of Firmicutes and Bacteroidetes instead of Proteobacteria, and highlight the importance of studying the microbiota in absolute terms.

Fecal microbiota transplants restore microbiota density and microbiota fitness

Given the large difference in the microbiota between healthy individuals and those with rCDI (Figure S5; Seekatz et al., 2014; Shankar et al., 2014), we hypothesized that on a mechanistic level, FMT bolsters colonization resistance by improving gut microbiota fitness. In fecal samples from FMT donors and their rCDI FMT recipients prior to and after FMT, we observed that the rCDI gut microbiota has a significantly lower microbiota density than the donor microbiota, and that FMT increased microbiota density ($p < 0.001$ for all comparisons, Tukey's HSD; Figure 5A). We did not observe any differences in fecal water content between the donors and recipients before or after FMT ($p > 0.2$ for all comparisons, Tukey's HSD). In addition, we found that rCDI FMT recipients had both a relative and absolute increase in Proteobacteria that was significantly reduced by FMT (Figures 5B, 5C, and S5C-S5F). These data suggest that FMT restores higher densities of Bacteroidetes, Firmicutes, and Actinobacteria to more fully realize the host's carrying capacity. However, several factors may confound this conclusion as individuals with rCDI are often on antibiotics prior to FMT and the disease is accompanied by severe diarrhea.

To separate the host physiologic and pharmacologic factors that might impact our understanding of community fitness in rCDI, we utilized a gnotobiotic murine model of FMT where germ-free mice were initially colonized with the fecal material of individuals with rCDI for 3 weeks prior to a single transplant of fecal material via oral gavage from a second human donor - the same healthy FMT donor used for the transplant clinically. As a control, we colonized germ-free mice with the second donor microbiota alone. The microbiota density of mice colonized with either healthy sample was greater than that of mice colonized with either rCDI sample ($p < 0.001$ for all comparisons, Tukey's HSD; Figure 5D), suggesting that rCDI individuals have a reduced microbiota fitness compared to healthy donors. Following FMT, we observed increases in microbiota density for both groups of mice ($p < 0.01$ for each, Tukey's HSD; Figure 5D), implying a restoration of microbiota fitness. These findings in the mice model recapitulated the data in our human cohort of FMT recipients and suggest that FMT successfully treats the fitness defect of the rCDI community.

Discussion

We found the density of gut microbes varies across mammals and is more similar in more phylogenetically related species. Gut architecture appears to be a major driver of density, as the lowest densities were observed in order *Carnivora*, whose short, simple intestines have a lower carrying capacity and are maladapted for microbial fermentation at high densities. Notably the low microbiota density of the red panda, a member of *Carnivora* with a herbivorous diet, as well as in humans with IPAA further support intestinal architecture as a major determinant of host carrying capacity and thus a driver of microbiota density.

Within a host with controlled carrying capacity, we found microbiota density can be altered both transiently and permanently with pharmacologics, with downstream consequences to host adiposity and immune function. Different antibiotics were highly varied in their ability to impact microbiota density, which could explain the mixed efficacy of antibiotics in microbiota-targeted clinical trials for complex disease and varied responses to antibiotics in animal models. Identifying more effective microbiota depleting cocktails would improve the design of such studies, while measuring microbiota density in trials with antibiotics could better stratify clinical response. Previous studies have observed that microbiota density and taxon survival can be manipulated by dietary cahnges (Llewellyn et al., 2017; Sonnenburg et al., 2016). Furthermore, we found that altering microbiota density with either diet or antibiotics could modify colitis severity (Llewellyn et al., 2017). Understanding the long-term effect of high or low microbiota density on health could help refine the use of diet and the microbiota in disease

treatment and prevention.

Finally, we observed that microbiota density is reduced in both IBD and rCDI. Microbiota density reductions, from lack of fitness in the microbial community, were “druggable” by FMT. The ability of FMT to increase microbiota density through improved community fitness provides mechanistic insights into FMT for rCDI and a novel biomarker to track its success. This result also highlights that routine monitoring to identify individuals with microbiota fitness deficiencies combined with prophylactic microbial therapeutics targeted might form a therapeutic strategy to boost colonization resistance and treat or prevent disease.

Acknowledgements

We are grateful to C. Fermin, E. Vazquez, and G. Escano in the Mount Sinai Immunology Institute Gnotobiotic facility for their help with gnotobiotic animal husbandry. D. Present provided helpful suggestions during the course of this work. Next generation sequencing was performed at NYU School of Medicine by the Genome Technology Center partially supported by the Cancer Center Support Grant, P30CA016087. Human microbiome processing was performed in part by the Human Immune Monitoring Center at the Icahn School of Medicine at Mount Sinai. This work was supported in part by the staff and resources of Scientific Computing and of the Flow Cytometry Core at the Icahn School of Medicine at Mount Sinai. Funding: This work was supported by grants from the Leona M. and Harry B. Helmsley Charitable Trust (I.D.), the NIH (NIGMS GM108505 for J.J.F. and NIDDK DK112679 for E.J.C.), Janssen Research & Development LLC, and SUCCESS.

Author Contributions

Conceptualization, E.J.C. and J.J.F.; Methodology, E.J.C., G.J.B., C.Y., I.M., Z.L., and S.R.L.; Formal Analysis, E.J.C; Investigation, E.J.C., G.J.B., and C.Y.; Resources, R.N., S.H., C.J., K.M.R., R.B., I.D., R.P.H., S.F., Y.L., N.Y., T.L., P.R.L., S.A.L., I.P., A.G., J.C.C., R.K., S.K., X.Q., A.C., A.H., A.A., J.R., F.F., M.Sa., A.N., P.Re., C.R., S.A., K.S., L.A.P., M.Su., R.H., K.H., J.Z., B.Z., B.L., H.I., W.S., A.D.N., W.W., B.L.C., C.D., D.G., S.I., A.L., J.M., E.M., R.U., S.N., J.N., B.Sh., T.U., P.Ru., J.G., P.L., S.E.T., J.R.F., J.C., J-F.C., C.B., S.P., E.S., C.A., M.D., A.K., B.Sa., and J.J.F.; Writing - Original Draft, E.J.C. and J.J.F.; Writing - Review & Editing, E.J.C., G.J.B., C.Y., I.M., C.J., K.M.R., A.G., J.C.C., L.A.P., H.I., S.I., S.E.T., J-F.C., A.K., J.J.F.; Visualization, E.J.C; Supervision, S.H., C.J., I.D., A.G., J-F.C., E.S., C.A., M.D., A.K., B.Sa., and J.J.F; Funding Acquisition, I.D., J-F.C., E.S., S.A.L., I.P., J.C.C., J.C., and J.J.F.

Declaration of Interests

B.C., R.H., M.D., and J.J.F. are consultants for Janssen.

Figures

Figure 1

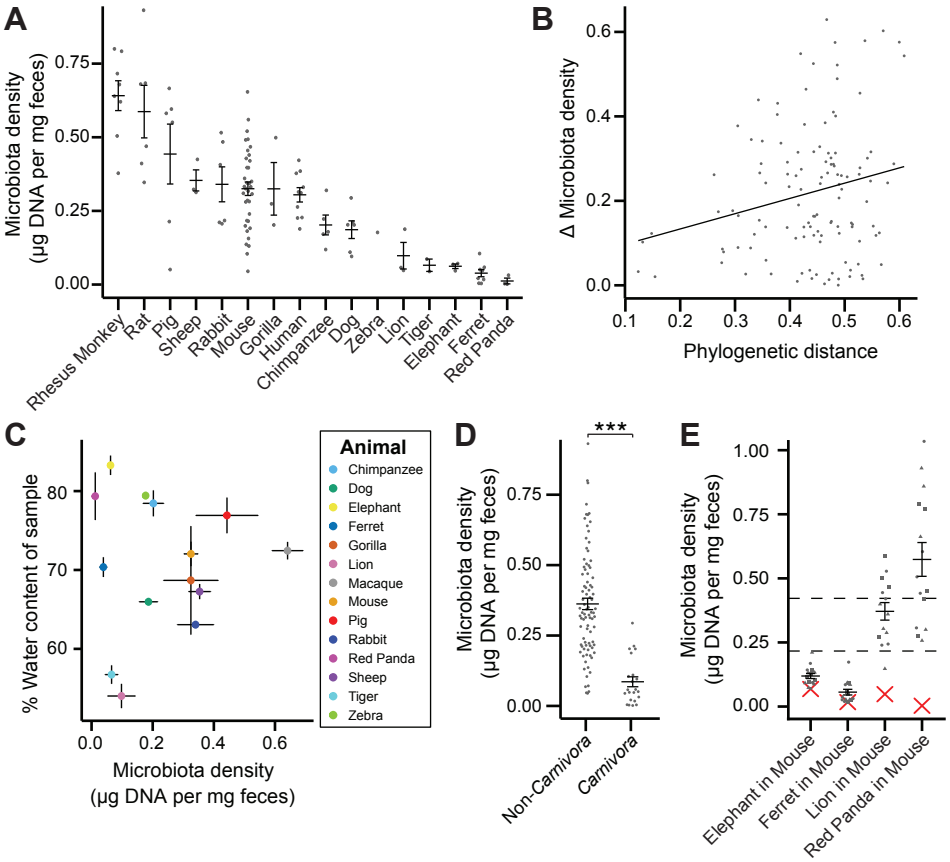

Figure 1. The natural variation in gut microbiota density across mammals is driven by host and microbial factors.

(**A**) Fecal microbiota density varies across mammals.

(**B**) Differences in microbiota density between animals was correlated with the degree of host phylogenetic relatedness as measured by mitochondrial 16S DNA sequence similarity.

(**C**) Microbiota density and water content of fecal samples are not correlated.

(**D**) Animals from the order *Carnivora* have a reduced microbiota density compared to mammals from other orders.

(**E**) Different mammalian gut microbiotas transplanted into germ-free Swiss Webster mice (n = 3 per group) vary in their fitness to reach densities similar to mouse microbiotas.

In **A** and **D-E**, points depict individual samples, and bars indicate mean ± SEM. In **C** points and lines indicate mean values ± SEM. In **E** a red *X* indicates the microbiota density of the original mammalian sample, while dashed lines represent IQR of conventional Swiss Webster mice. ***p < 0.001.

Figure 2

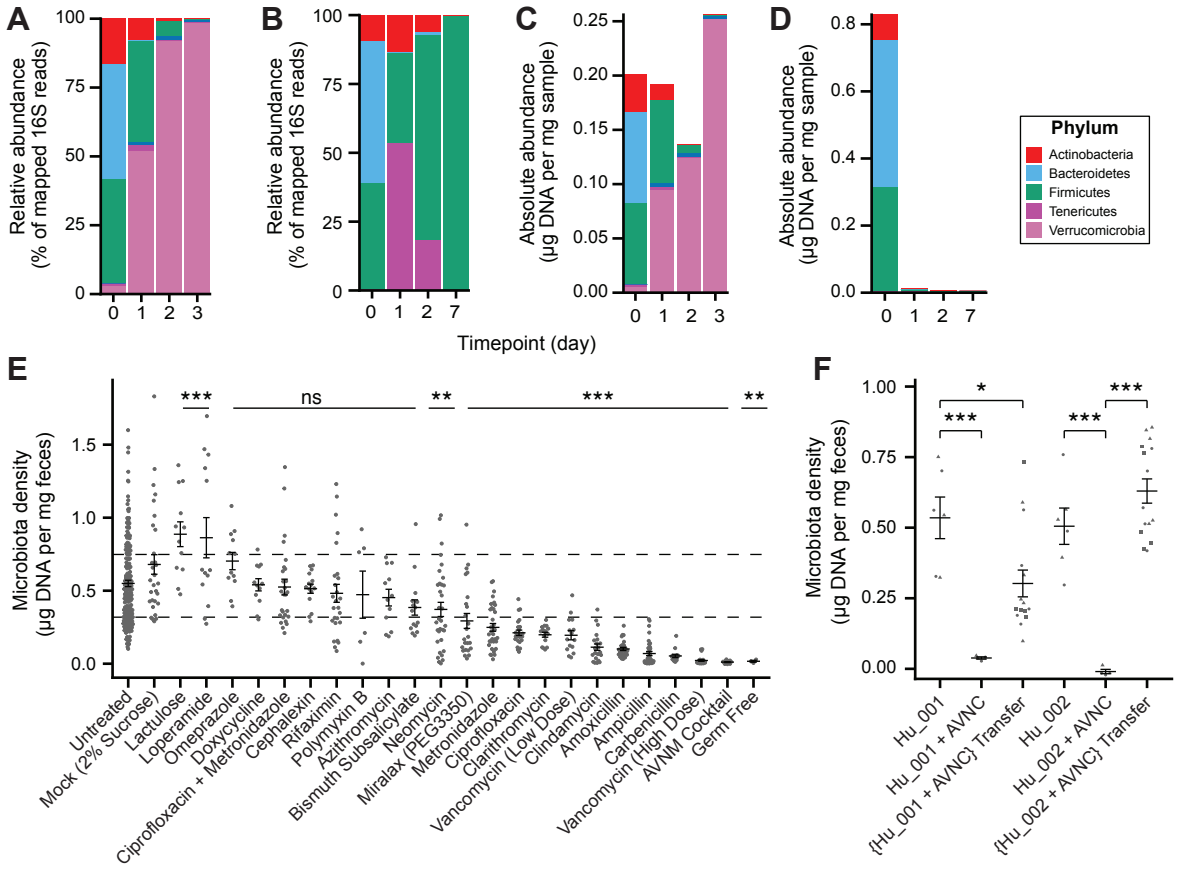

Figure 2. Alteration of the absolute murine fecal microbiota by pharmacologics.

(**A-D**) The relative abundances of the microbiota in SPF C57BL/6J mice treated with (**A**) low dose (n = 5) and (**B**) high-dose (n = 3) vancomycin are each dominated by a single phyla. Taking changes in microbiota density into account, the absolute abundance of the microbiota at the phylum level in the (**C**) low-dose vancomycin group demonstrates an expansion of Verrucomicrobia compared to reduction of all phyla in the (**D**) high-dose vancomycin group.

(**E**) Pharmacologic interventions differentially alter microbiota density in SPF C57BL/6J mice. Samples from 3-12 (mean = 6) mice per group.

(**F**) Microbial density in germ-free Swiss-Webster mice (n = 2 mice per group) colonized with one of two healthy human fecal samples (Hu_001, Hu_002) decreased upon treatment with the AVNC antibiotic cocktail. The Hu_001 AVNC-treated microbiota had decreased fitness upon transfer into germ-free mice (n = 3 per group).

In **E**, dashed lines represent the IQR of untreated SPF C57BL/6J mice and AVNM = ampicillin, vancomycin, neomycin, metronidazole. Statistical tests performed for individual treatment conditions vs untreated using Dunnett's test. In **E** and **F**, bars indicate mean ± SEM. In **F**, points represent individual samples and shapes represent mice and AVNC = ampicillin, vancomycin, neomycin, clindamycin. Statistical comparisons performed with Tukey's HSD to correct for multiple comparisons. ns = not significant, *p < 0.05, **p < 0.01, and ***p < 0.001. See also Figure S2.

Figure 3

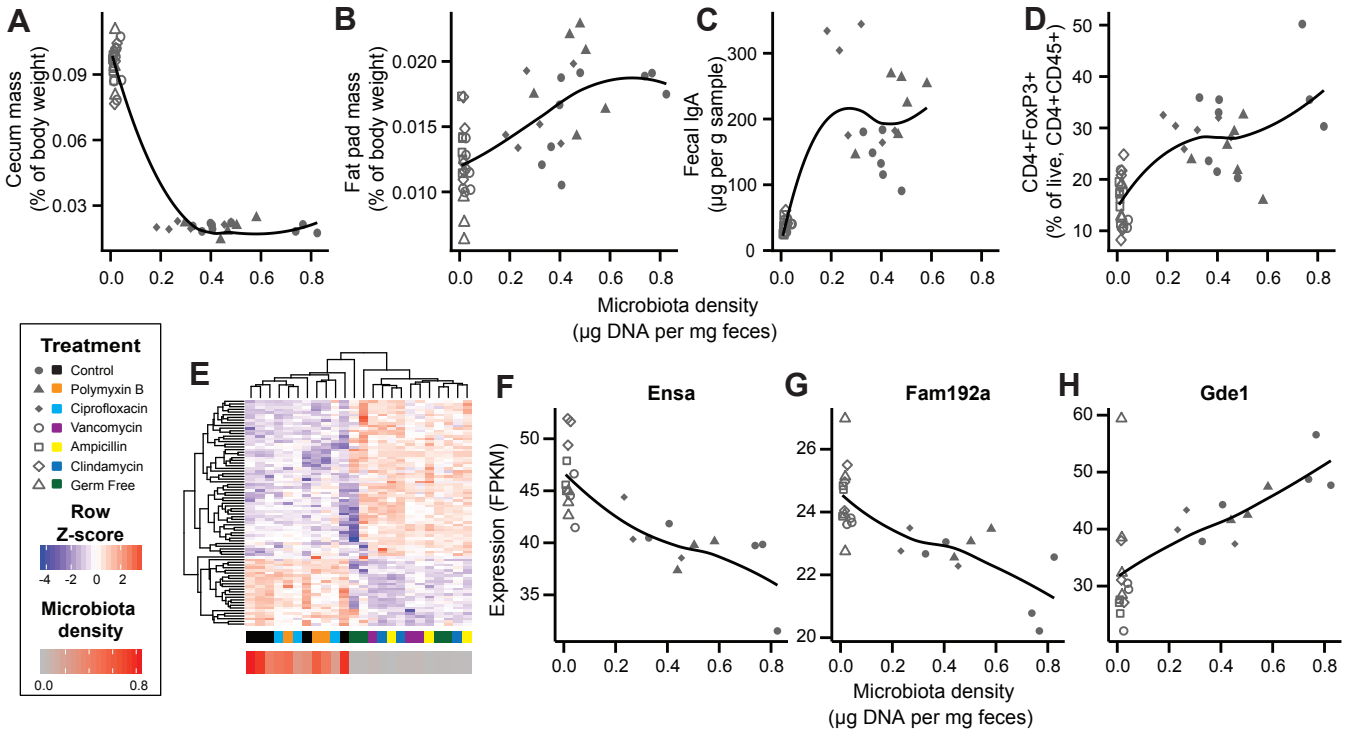

Figure 3. Manipulation of colonic microbiota density alters host physiology.

(**A-D**) Antibiotic-induced changes in microbiota density significantly correlate with (**A**) host cecum size, (**B**) adiposity, (**C**) fecal IgA, and (**D**) colonic lamina propria FoxP3+ T regulatory cells. n = 6 mice per antibiotic group, 9 SPF antibiotic-free controls, and 6 germ-free controls.

(**E**) Expression and clustering of transcripts correlated with microbiota density reveals two clusters defined by microbiota density depletion.

(**F-H**) *Ensa*, *Fam192a*, and *Gde1* expression are highly correlated with microbiota density.

In **A-D** and **F-H**, points represent individual mice. Shapes indicate treatment group. Curves were fit using LOESS regression.

In **E**, colored bars below the heatmap represent the treatment group and microbiota density. See also Figure S3.

Figure 4

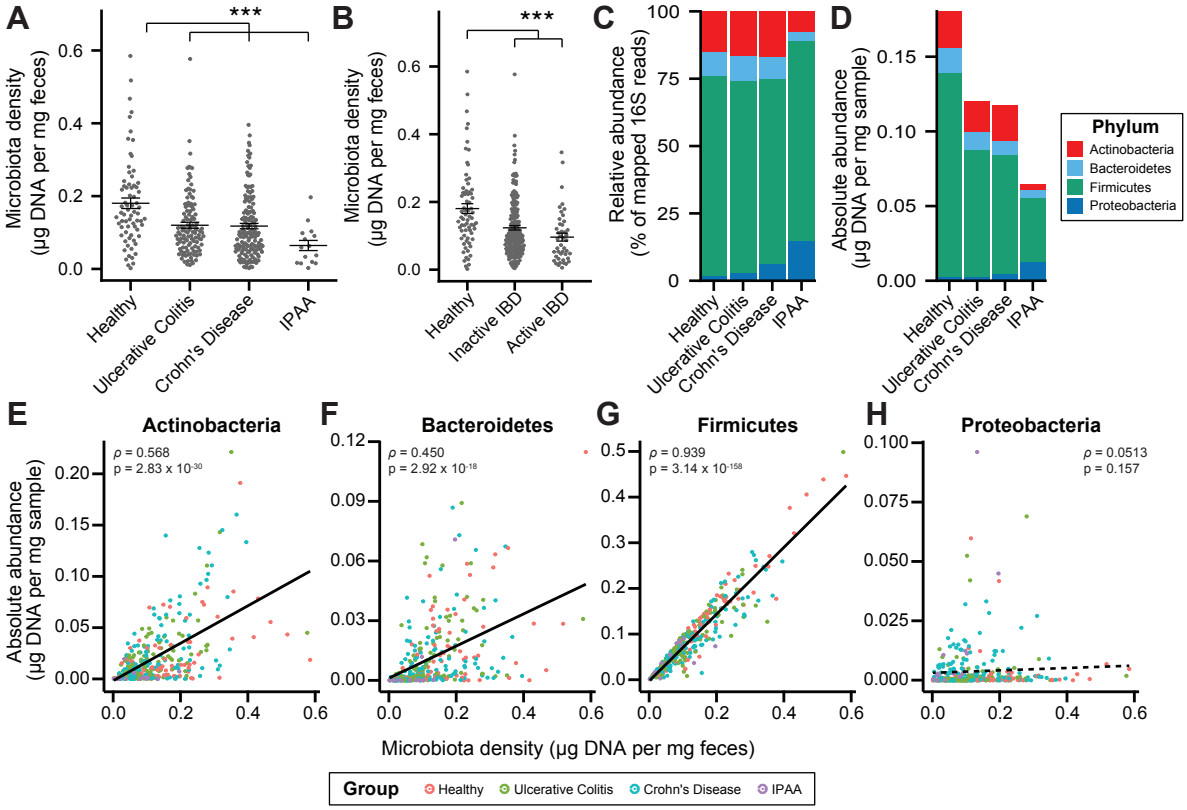

Figure 4. Differences in the absolute microbiota of individuals with IBD.

(**A**) Subjects with ulcerative colitis and Crohn's disease, as well as subjects who have undergone ileal pouch-anal anastomosis (IPAA) have reduced microbiota density compared to healthy controls.

(**B**) The reduction in microbiota density in IBD patients is independent of disease activity.

(**C-D**) 16S rRNA sequencing reveals phylum-level changes in (**C**) relative and (**D**) absolute abundances of the microbiota in subjects with UC, CD, and IPAA compared to healthy controls.

(**E-H**) The absolute abundance of all of the major phyla are strongly correlated with microbiota density, with the exception of Proteobacteria, whose abundance is largely constant.

In **A** and **B**, bars indicate mean ± SEM, and *** $p < 0.001$ (Tukey's HSD). In **E-H**, points represent individual subjects and colors indicate their health status. See also Figure S4.

Figure 5

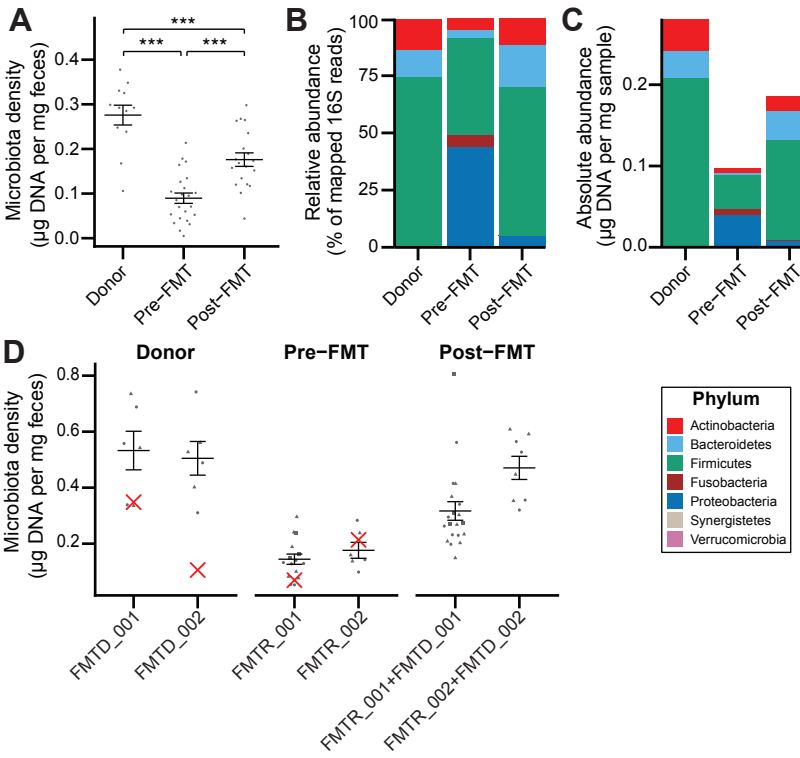

Figure 5. Changes in absolute microbiota in individuals with rCDI following FMT.

(**A**) rCDI subjects have reduced microbiota densities that are significantly increased upon FMT with donor microbiotas. (**B** and **C**) Following FMT, the composition of the microbiota of individuals with rCDI is restored to more closely resemble that of healthy donors in both (**B**) relative and (**C**) absolute terms.

(**D**) Microbial density in a mouse model of FMT (n = 3 for recipient mice, n = 2 for donor mice) using multiple donor-recipient pairs show an increase in microbiota density following FMT, suggesting a restoration of community fitness.

In **A**, points represent individual samples, bars indicate mean ± SEM, and ***p < 0.001 (Tukey's HSD). In **D**, shapes indicate individual mice and the red *X* indicates the microbiota density of the original mammalian sample. See also Figure S5.

Methods

Experimental Model and Subject Details

Mammalian samples

Fecal samples from the mammals used in this study were collected either from laboratory animals housed and maintained at the Icahn School of Medicine at Mount Sinai (New York, NY), or from animals at the Knoxville Zoo (Knoxville, TN).

Mice

Specific pathogen free (SPF) mice were purchased from Jackson Labs (C57BL/6J mice) or Taconic (Swiss Webster mice). Germ-free (GF) WT C57BL/6J and Swiss Webster mice were housed in standard, commercially available flexible film isolators. To generate gnotobiotic mice from human or mammalian fecal samples, GF mice were gavaged with 200 μL of clarified stool from the source. Four week old male mice were used for the antibiotic treatment phenotyping experiments (Figure 3). All other experiments used both male and female mice between 4 and 6 weeks old. Swiss Webster mice were used to perform gnotobiotic experiments. Experiments and animal care were performed in accordance with the policies of the Icahn School of Medicine Institutional Animal Care and Use Committee (IACUC).

Human subjects

To study the microbiota of individuals with IBD, we collected fecal samples from 70 healthy controls (42 female, 28 male), with an average age of 55.1 (range: 23-73), 109 individuals with ulcerative colitis (67 female, 42 male), with an average age of 52.8 (range: 22-80), and 144 individuals with Crohn's Disease (72 female, 72 male), with an average age of 41.7 (range: 22-79). The study was approved by the Institutional Review Board (IRB) at Mount Sinai. For subjects with ulcerative colitis we defined disease activity using the Mayo Endoscopic Subscore (Mayo). Individuals with a Mayo = 3 were categorized as having active disease, and individuals with a Mayo = 0 were categorized as having inactive disease. For individuals with Crohn's disease, active disease was defined as a Simple Endoscopic Score for Crohn Disease (SES-CD) $\geq$ 5, and inactive disease as SES-CD = 0. The remaining samples were excluded from these analyses. Stool samples were also collected from individuals with ulcerative colitis that had undergone an ileal pouch-anal anastamosis procedure following total colectomy (3 female, 12 male), with an average age of 42.93 (range: 19-68). These samples were collected from individuals in accordance with the IRB at the Tel Aviv Sourasky Medical Center. All individuals signed an informed consent. For the analysis of the change in the microbiota in recurrent *Clostridium difficile* infection following fecal microbiota transplantation, we collected samples from 11 healthy donors (8 female, 3 male; average age: 47.9, range: 25-75), 12 recipients who also had IBD (8 female, 4 male; average age: 55.3, range: 32-78), and 11 recipients who did not have IBD (9 female, 3 male; average age: 62, range: 36-87), as described in (Hirten et al., 2018). The study was approved by the Mount Sinai IRB.

Method Details

Fecal sample collection and pre-processing

To quantify the mass of each fecal sample or fecal sample aliquot, we pre-weighed tubes prior to sample collection and post-weighed the tubes after adding the fecal material. For mouse samples, fresh fecal samples were collected directly into the collection tubes and stored at -80°C. For all other mammalian species with larger fecal sample sizes, samples were

aliquoted on dry ice or liquid nitrogen and stored at -80°C. Sample aliquot sizes were targeted in the linear range of the fecal DNA extraction protocol (approx. 50 mg in mice and <200 mg in humans) to enable quantitative yields of DNA from the fecal material.

Phenol:chloroform DNA extraction

Fecal samples processed with the phenol:chloroform DNA extraction method were collected into 2.0 mL collection tubes (Axygen, SCT-200-SS-C-S). Similar to previous studies (Reyes et al., 2013), samples were suspended in a solution containing 282 μL of extraction buffer (20 mM Tris (pH 8.0), 200 mM NaCl, 2mM EDTA), 200 μL 20% SDS, 550 μL phenol:chloroform:isoamyl alcohol (25:24:1, pH 7.9), and 400 μL of 0.1 mm diameter zirconia/silica beads (BioSpec, 11079101z). Samples were then lysed by mechanical disruption with a Mini-Beadbeater-96 (BioSpec, 1001) for 5 minutes at room temperature. Samples were centrifuged at 4000rpm for 5 minutes to separate aqueous and organic phases. The aqueous phase was collected and mixed with 650 μL of PM Buffer (Qiagen, 19083). DNA extracts were then purified using a Qiagen PCR Purification kit (Qiagen, 28181), and eluted into 100 μL of EB buffer. Purified DNA was quantified using the Broad Range or High Sensitivity Quant-IT dsDNA Assay kit (Thermo Fisher, Q32853 and Q33130) in combination with a BioTek Synergy HTX Multi-Mode Reader.

DNase Inactivation Buffer DNA extraction

Phenol:chloroform based DNA extraction with bead beating is an effective method to isolate microbial DNA from feces. However, automation of phenol:chloroform requires liquid handling robotics in an environment compatible with this hazardous chemical mixture. In addition, the variable volume of the aqueous phase produced with this method presents an obstacle for its automation. We therefore tested the DIB bead beating extraction protocol as an alternative, since by eliminating the hazardous chemicals the protocol is compatible with more high-throughput liquid handling robotics platforms.

Samples processed with the DNase Inactivation Buffer (DIB) DNA extraction method were collected into 1.0 mL tubes (Thermo Fisher, 3740). Samples were suspended in a solution containing 700 μL of DIB (0.5% SDS, 0.5 mM EDTA, 20 mM Tris (pH 8.0)) and 200 μL of 0.1 mm diameter zirconia/silica beads. Samples were then lysed by mechanical disruption and centrifuged as above. Since there is no phase separation with this method, it is straightforward to subsample the supernatant to improve the dynamic range of DNA quantification by avoiding saturating the column with DNA quantities above the binding capacity. 50-200 μL of the supernatant was transferred into new collection tubes. Depending on the volume collected, an additional volume of DIB was added in order to reach a total volume of 200 μL. Next, this DIB lysate was combined with 600 μL of PM Buffer, purified with a Qiagen PCR Purification kit, and eluted into 100 μL of EB buffer. Purified DNA was quantified using the Broad Range or High Sensitivity Quant-IT dsDNA Assay kit in combination with a BioTek Synergy HTX Multi-Mode Reader.

To test if the two DNA extraction methods affected the resulting microbiota composition data, we processed separate aliquots from the same fecal sample using both methods. We found that the abundances of taxa in the sample processed with both methods were highly correlated (Figures S1A and S1B), suggesting that they represent equivalent ways to assay microbial community composition. In practice, the DIB method was most conducive to the small feces produced by mice and the large majority of mouse samples for this study were processed using this protocol, since the protocol utilizes smaller tubes that can be arrayed into standard 96-well formats. For the remaining mammals, the phenol:chloroform method was used as the number of stools used in the study was less, and the larger stools were more practical to aliquot into the wider

2.0 ml tube used for the phenol:chloroform method.

One possible limitation of using DNA content as a measurement of microbiota density is that small amounts of fecal matter contain sufficient DNA to saturate or clog the DNA binding columns used during extraction. This upper limit can largely be avoided by limiting the amount of input fecal material of higher microbiota density mammals (*e.g.* mice) to <50 mg and lower microbiota density mammals (*e.g.* humans) to <200 mg. In our experience, bead beating also becomes inefficient at >200 mg of fecal material. In contrast to the phenol:chloroform method, the DIB extraction protocol relies on a subsampling step that provides an additional safeguard to ensure the DNA extraction does not saturate the capacity of the Qiagen DNA-binding columns. By sampling a fraction of the lysate, we can extend the upper limit of our extraction protocol. At the extreme, using a 5 μL subsample of the lysate can increase the dynamic range by a factor of 140, which in turn implies that we can measure microbiota density for samples containing up to 1.4 mg of DNA (140 x 10 μg binding capacity of columns). On the lower end of our dynamic range, dye-based methods (Qubit Hi-sensitivity) provide an accurate detection down to 0.2 ng.

qPCR quantification of DNA origin

While the dynamic range of the DIB extraction method described above is typically sufficient for stool samples, which contain high densities of microbial DNA compared with other environments, we further extended the method with qPCR-based quantification of the V4 region of the 16S rRNA region. Additionally, by utilizing DNA yield per fecal sample as a measure of microbiota density, we assume host DNA is a minor contributor to the total fecal DNA yield.

To quantify the amount of bacterial and mouse DNA in our samples, we targeted the V4 region of the bacterial 16S rRNA gene (Relman et al., 1992) and the mouse TNFα gene (Nitsche et al., 2001). qPCR reactions were performed in 20 μL reaction volumes with final primer concentrations of 200 nM, using KAPA SYBR FAST Master Mix (2x) ROX Low (Kapa Biosystems). The thermal cycling and imaging were performed on the ViiA 7 Real-Time PCR System (Thermo Fisher).

We quantified the amount of host vs bacterial DNA in several samples by qPCR, and evaluated the qPCR performance against spike-in controls with known combinations of mouse and bacterial DNA. We found that even amongst samples with low microbial density (e.g. samples from mice treated with vancomycin), the DNA content is largely microbial (Figure S1C). We were also able to measure the presence of microbial DNA down to concentrations near 1 pg/μL (Figure S1C). This allows us to measure microbial density for samples with DNA as low as 100 pg (minimum concentration 1 pg/μL in a 100 μL elution volume). Coupled with the ability to subsample the lysate from our DNA extraction protocol, this allows us to measure microbiota density across 5 orders of magnitude for the phenol:chloroform method and 7 orders of magnitude with the DIB protocol.

16S rRNA sequencing

DNA templates were normalized to 2 ng/μL, and the V4 variable region of the 16S rRNA gene was amplified by PCR using indexed primers as previously described (Faith et al., 2013). The uniquely indexed 16S rRNA V4 amplicons were pooled and purified with AmpureXP beads (Beckman Coulter) with a ratio of 1:1 beads to PCR reaction. Correct amplicon size and the absence of primer dimers were verified by gel electrophoresis. The pooled samples were sequenced with an Illumina MiSeq (paired-end 250bp).

Fecal sample water content

Samples were collected into pre-weighed 2.0 mL collection tubes (Axygen, SCT-200-SS-C-S). After collecting a fecal sample, sample mass was determined by post-weighing the tube. To measure the water content of a sample, tubes were placed at 105°C for 24 hours, and weighed again (Hinnant and Kothmann, 1988). The water content of a sample was calculated as the difference in final and initial mass of the sample, divided by the initial mass.

Pharmacologic treatment of mice

Antibiotics (and other compounds) were provided *ad libitum* to mice in their drinking water, when possible. All of the pharmacologics were prepared into a 2% sucrose solution (which also served as the control treatment) and sterilized with a 0.22 μm filter. Compounds that were not readily water-soluble were administered to mice via oral gavage of 200 μL once per day, as indicated in Table S2. Unless identified otherwise, antibiotic and pharmacologic concentrations were calculated using a maximal clinical dose (taken from the online clinical resource UpToDate.com) or from previous studies (Atarashi et al., 2011; Bryant et al., 1988; Kashyap et al., 2013; Larsson et al., 1983; Vaishnava et al., 2011), assuming a 20 g mouse that drinks 3 mL water per day.

Measurement of fecal immunoglobulin A

Fecal pellets were collected and massed. To each fecal pellet, 1 mL of sterile PBS was added per 100 mg feces. Each sample was homogenized without beads in a Mini-Beadbeater-96 for 3 min (BioSpec, 1001) followed by vortexing for 3 min. Samples were centrifuged at 9000g for 10 min at 4°C and supernatants were collected. Immunoglobulin A was measured by ELISA. Plates were coated with a working concentration of 1 ng/μL of goat anti-mouse IgA-UNLB (SouthernBiotech Cat# 1040-01, RRID:AB_2314669), and then blocked with 1% BSA in PBS overnight at 4°C. Wells were washed with washing buffer (0.1% Tween-20 in PBS) 3 times. Then fecal supernatant was diluted in dilution buffer (0.1% Tween-20, 1% BSA in PBS), added to each well, and incubated overnight at 4°C. The wells were washed again with washing buffer 5 times, and incubated for 2 hours at room temperature with a 1/2000 dilution of goat anti-mouse IgA-HRP (Sigma-Aldrich Cat# A4789, RRID:AB_258201) in dilution buffer. Following the incubation, the wells were washed 5 times with PBS/Tween-20. Next, TMB substrate was added to wells for 1 minute (KBL, 50-76-02 and 50-65-02), and the reaction was quenched using 1M H_2SO_4. Absorbance at 450 nm was measured using a BioTek Synergy HTX Multi-Mode Reader. Samples were quantified against a standard curve from 1000 ng/mL to 0.5 ng/mL.

Colonic lamina propria immune populations

Colonic lamina propria immune cell populations were measured as previously described (Britton et al., 2018). Briefly, colonic tissue was dissected and placed into RPMI medium at 4°C. Tissues were then transferred into HBSS and vortexed briefly, before being transferred into dissociation buffer (10% FBS, 5 mM EDTA, 15 mM HEPES in HBSS) and shaken for 30 minutes at 110 rpm at 37°C. Tissues were washed in HBSS before digestion in HBSS containing 2% FBS, 0.5 mg/mL Collagenase VIII (Sigma C2139) and 0.5 mg/mL DNase 1 (Sigma DN25) for 30 minutes at 110 rpm at 37°C. Digested tissue was then passed through a 100 μm filter into cold RPMI medium. Samples were then centrifuged at 1500 rpm, 4°C for 5 minutes. The supernatant was removed and cells were washed once more in PBS before staining for flow cytometry. No enrichment of mononuclear cells by density centrifugation was performed. Cells were initially blocked with Fc Block (BioLegend Cat# 101320, RRID:AB_1574975) and subsequently stained for: viability (BioLegend Cat# 423101) and immunolabelled for expression

of CD4 (1:200, BioLegend Cat# 100411, RRID:AB_312696) and CD45 (1:100, BioLegend Cat# 103115, RRID:AB_312980), and FoxP3 (1:100, Thermo Fisher Scientific Cat# 12-5773-82, RRID:AB_465936). Surface markers were stained before fixation and intracellular markers were stained after fixation with the FoxP3 Fixation/Permeabilization Kit (eBioscience). Samples were run on a BD LSRII and analyzed with FlowJo.

RNA extraction and sequencing

Samples were processed as previously described in Llewellyn et al. (2017). Briefly, approximately 0.5 cm of the proximal colon was taken for RNA extraction and sequencing. Samples were collected into 500 μL of RNAlater Stabilization Reagent (Qiagen, 76104) and placed at 4°C overnight. Then, samples were transferred to -80°C for storage until RNA extraction. Total RNA was extracted from samples using a Qiagen RNeasy Mini Kit (Qiagen, 74104). Tissue homogenization was performed by bead beating using 250 μL of 1.0 mm Zirconia/Silica beads in 1.5 mL of RLT Buffer + 1% β-meracaptoethanol. RNA quality was assessed using the Agilent Bioanalyzer 6000 Nano Kit (Agilent, 5067-1511). mRNA Illumina libraries were generated by the NYU Genome Technology Center and sequenced on an Illumina HiSeq to a depth of 27.6 ± 5 million 50 nt paired-end reads per sample.

Quantification and Statistical Analysis

Microbiota density and absolute abundances

We define microbiota density as the total DNA extracted from each sample (in μg) per mg of fresh sample. For samples processed with the DIB-based extraction method, the total DNA extracted is adjusted by the fraction of the supernatant that was subsampled in the DNA extraction (e.g. a 100 μL subsample is 1/7th of the total volume; total sample DNA is [DNA eluted] * 7). We then are able to utilize this measurement of microbiota density to compute the absolute abundance of microbial taxa by scaling the relative abundances of microbes in a sample by the microbiota density of that sample.

Phylogenetic relatedness of mammalian samples

Phylogenetic relatedness was measured using sequence distance of the mitochondrial DNA sequences. All sequences were downloaded from the RefSeq organelle genome resource database (https://www.ncbi.nlm.nih.gov/genome/organelle/). Accession numbers for specific sequences used can be found in Table S1. Sequence alignment and distance measurement was performed using Clustal Omega (Sievers et al., 2011).

16S rRNA data analysis

Paired end reads were joined into a single DNA sequencing using the FLASH algorithm (Magoč and Salzberg, 2011). We split our pooled sequencing library by index using QIIME (v 1.9.1) (Caporaso et al., 2010), and picked OTUs against the greengenes reference database 13_8 at 97% sequence identity (DeSantis et al., 2006; McDonald et al., 2012). The resulting OTU tables were subsequently analyzed in R (R Core Team, 2017) with the help of the *phyloseq* package (McMurdie and Holmes, 2013), and custom functions developed to convert relative abundances into absolute abundances using microbiota density data.

RNA sequencing data analysis

Transcript expression values were obtained by mapping to the Mus musculus mm10 genome (http://genome.ucsc.edu/) using HISAT (Kim et al., 2015; Pertea et al., 2016) and StringTie (Pertea et al., 2015). Gene expression was determined and analyzed with the *ballgown* R package (Frazee et al., 2015).

Statistical Analysis

Data presented were analyzed and visualized using the R statistical software (R Core Team, 2017). Statistical tests were used as described in the main text. For many-to-one comparisons (e.g. pharmacologic treatments compared to untreated controls), multiple hypothesis testing correction was accomplished by using Dunnett's test, implemented with the *multcomp* R package (Hothorn et al., 2008). For multiple comparisons between experimental groups, Tukey's honest significant difference (HSD) was used to correct for multiple testing. Unless otherwise noted, figures depict individual samples as points, and the bars indicate the mean $\pm$ SEM. In figures, *p < 0.05, ** p < 0.01, and ***p < 0.001.

Repeated sampling of gnotobiotic mice

For the experiments in which gnotobiotic mice were used to assess the roles of host carrying capacity and microbiota fitness in shaping microbiota density, mice were sampled longitudinally to increase sample size for each condition. For the mice colonized with fecal samples from the lion, elephant, ferret, and red panda, two-way ANOVA shows that the main effect is the microbiota used to colonize the mouse ($F = 32.3$, $p = 8.27 \times 10^{-16}$), while the identity of the individual mice does not contribute to the effects ($F = 1.08$, $p = 0.388$). The same is true for the mice colonized with fecal samples from individuals with IBD and pouch ($F = 29.4$, $p < 0.0001$ for the colonizing microbiota; $F = 0.746$, $p = 0.634$; two-way ANOVA). As a result, we are able to effectively measure the microbiota density of gnotobiotic mice in these conditions and increase the utility of each gnotobiotic mouse.

Data and Software Availability

Raw sequencing files (fastq) for all 16S sequencing samples (antibiotic-treated mice, IBD cohort, and rCDI FMT cohort) are stored in the public Sequence Read Archive (SRA) under project number PRJNA413199. The RNA sequencing data (antibiotic-treated mice) have been deposited in NCBI's Gene Expression Omnibus (GEO) (Edgar et al., 2002) and are accessible through GEO Series accession number GSE104871.

Supplemental Items

Supplemental figures

Figure S1

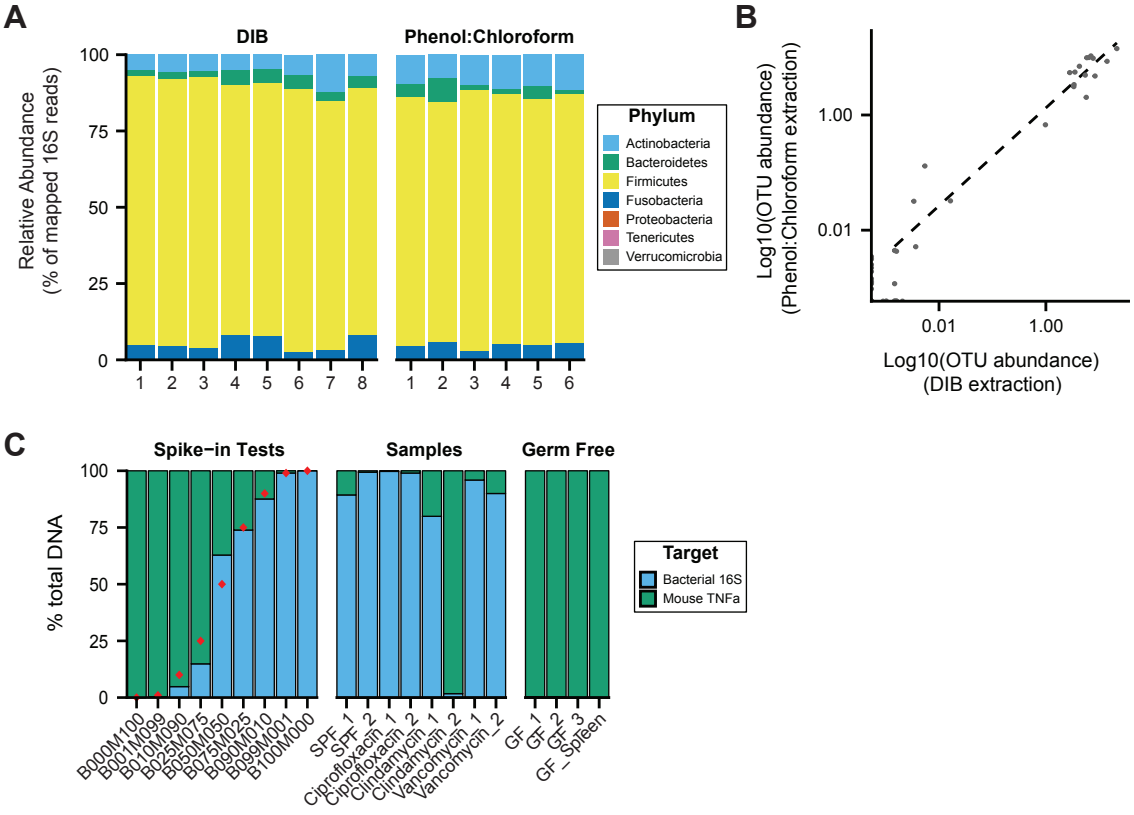

Figure S1. Related to Methods. DNAse Inactivation Buffer DNA extraction method (DIB) does not alter microbiota community composition compared to phenol:chloroform extraction and extracts DNA that is largely bacterial in origin.

We homogenized one dog fecal sample and created multiple aliquots for DNA extraction using either the DIB or phenol:chloroform extraction methods.

(**A**) We do not observe evidence of bias introduced by the DNA extraction method chosen, as we observe similar microbial compositions for the multiple aliquots, regardless of extraction method.

(**B**) Relative OTU abundances from these samples are highly correlated across the two extraction methods (ρ = 0.904, p = 1.82 x 10^{-45}, Pearson's correlation). Dots represent average values of an individual OTU abundance across several aliquots processed using each method (n = 8 for DIB, n = 6 for phenol:chloroform).

(**C**) We performed qPCR of host and bacterial fractions of mixed mouse/microbial DNA samples. Spike-in samples with known fractions of mouse and bacterial DNA (*e.g.* B010M090 = 10% bacterial + 90% mouse) were quantified with qPCR to validate the potential to identify the origin of DNA in a mixed sample. Samples from mouse fecal pellets across a variety of conditions show that the host contribution to the extracted DNA is small, even for samples with low microbiota density. Red points indicate the true spike-in percentage of bacterial DNA. GF_1, GF_2, GF_3 are host DNA controls of germ-free mouse feces. GF_Spleen is a host DNA control from a germ-free mouse spleen.

Figure S2

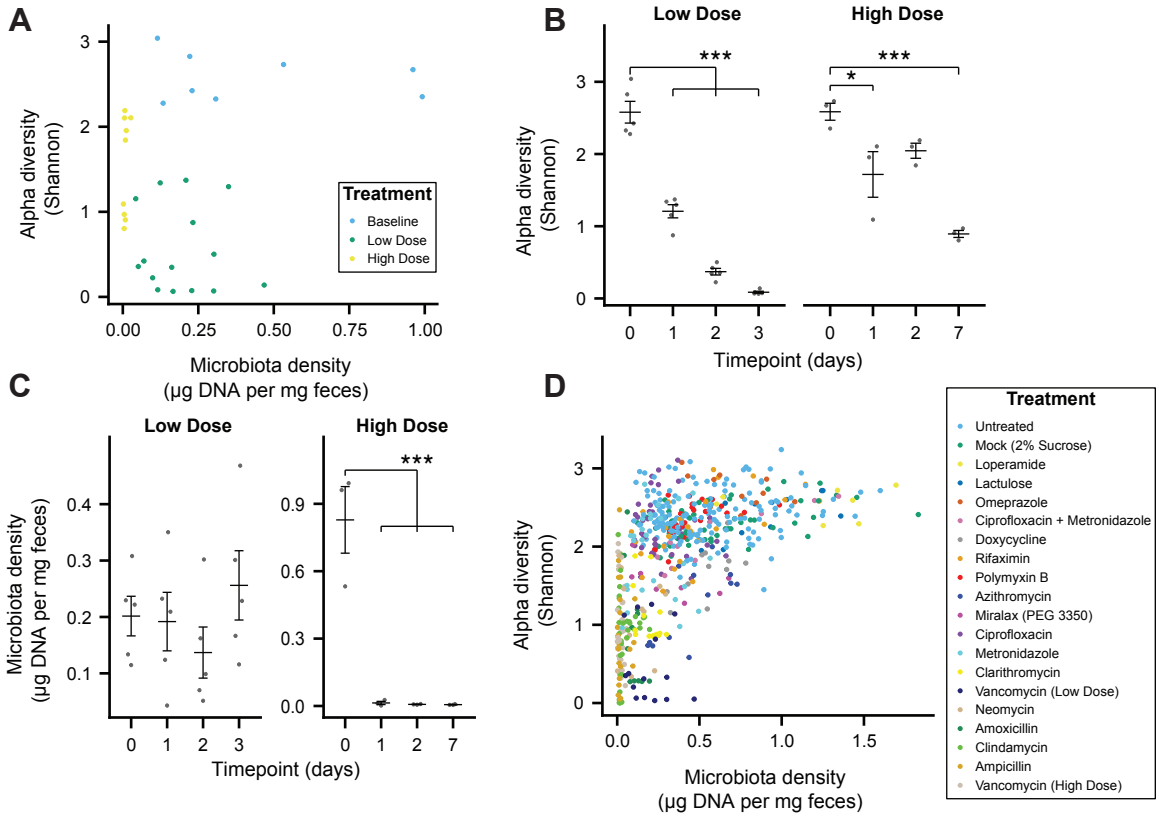

Figure S2. Related to Figure 2. Low versus high dose vancomycin treatment causes different disruptions of the absolute microbiome.

(**A**) Changes in alpha diversity in response to high (0.5 mg/mL, n = 3) and low (0.2 mg/mL, n = 5) dose vancomycin treatment do not correlate with the changes observed in microbiota density.

(**B**) Both low and high dose vancomycin treatment in mice reduce alpha diversity ($p = 1.56 \times 10^{-7}$, $p = 0.0161$, respectively, vs baseline; Dunnett's test).

(**C**) Low dose vancomycin did not significantly alter microbiota density, while high dose vancomycin reduced microbiota density to near zero ($p = 0.910$, $p = 8.61 \times 10^{-7}$, respectively, vs baseline; Dunnett's test).

(**D**) Across all conditions, we never observe high microbiota density with low alpha diversity, which drives a significant correlation between alpha diversity and microbiota density ($\rho = 0.628$, $p < 0.0001$, Spearman correlation). However, we commonly observe high alpha diversity with low microbiota density (e.g. animals given metronidazole), again suggesting the changes in microbiota density do not strictly correspond to changes in alpha diversity.

In **A** and **B**, bars indicate mean $\pm$ SEM, *p < 0.05, and ***p < 0.001. In **C** and **D**, points represent individual samples and colors indicate treatment.

513 **Figure S3**

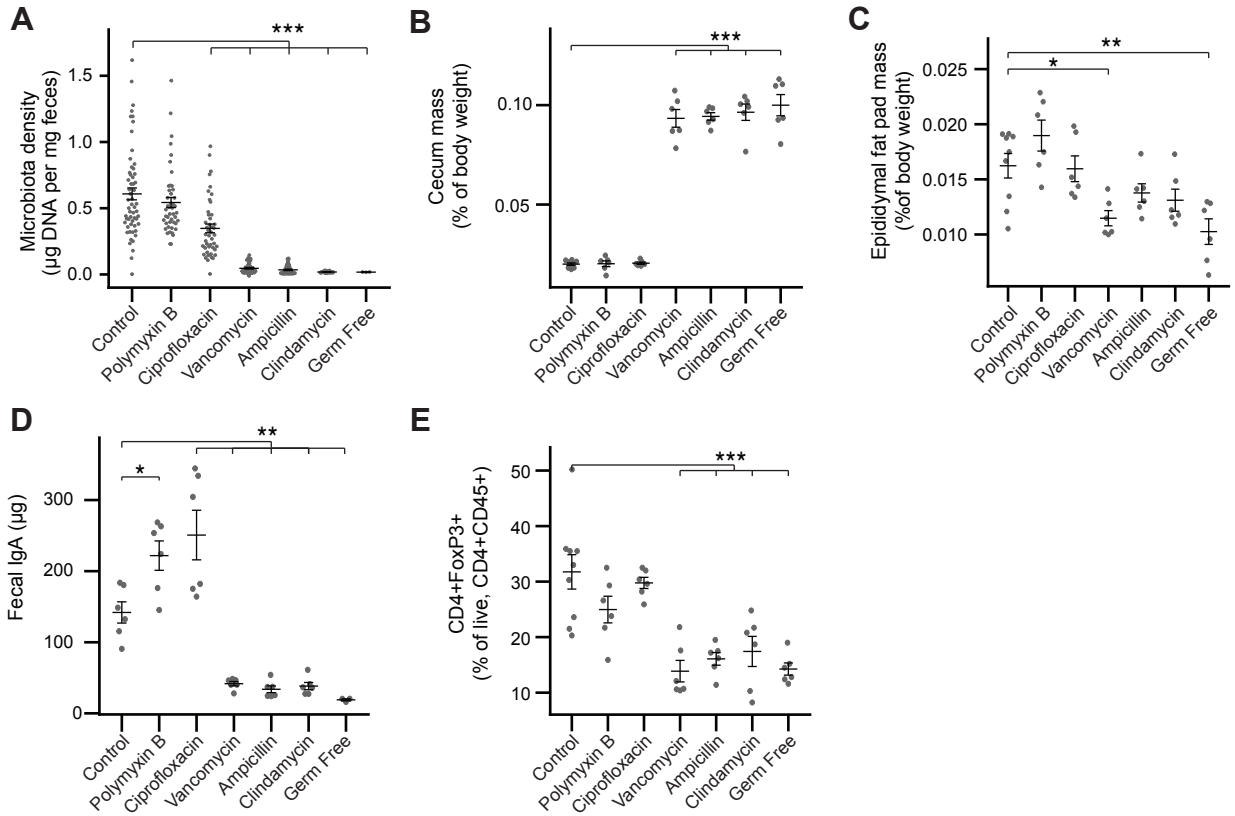

514

515 **Figure S3. Related to Figure 3. Phenotypic changes observed in antibiotic-treated mice.**

516 (**A**) Microbial density changes observed in mice administered antibiotics *ad libitum* in drinking water for four weeks.

517 (**B-E**) The reduction in microbiota density results in changes in the (**B**) cecum size, (**C**) epididymal fat pad mass, (**D**) fecal

518 IgA, and (**E**) colonic lamina propria FoxP3+ T regulatory cells.

519 Bars indicate mean ± SEM. *p < 0.05, **p < 0.01,***p < 0.001 (Dunnett's test)

Figure S4

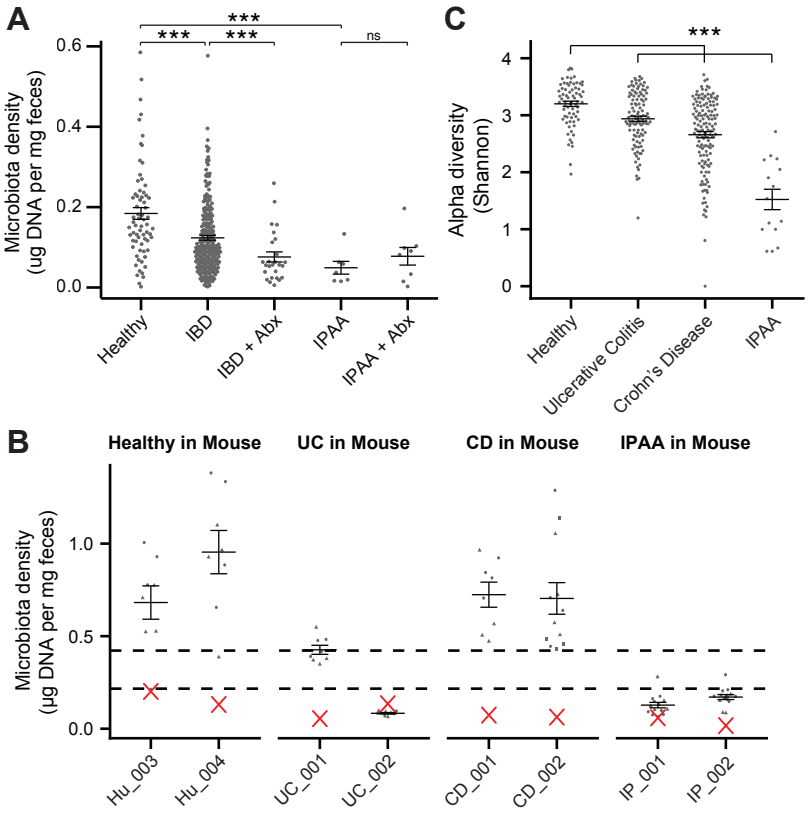

Figure S4. Related to Figure 4. The microbiota of IBD and IPAA subjects

(**A**) Microbiota density is reduced in subjects with IBD and IPAA in the absence of antibiotic use. Nonetheless, the microbiota density of individuals with IBD on antibiotics was significantly lower for individuals with IBD on antibiotics.

(**B**) Microbial density in germ free Swiss-Webster mice colonized with Healthy (Hu_003, Hu_004), IBD (UC_001, UC_002, CD_001, CD_002), or IPAA patient fecal samples (IP_001, IP_002) have different densities suggesting a range of microbial fitness across microbiotas with IPAA microbiotas being the least fit.

(**C**) Alpha diversity is reduced in subjects with IBD relative to healthy controls

In **A-C**, bars indicate mean ± SEM. ***p < 0.001, ns = not significant. In **B**, dashed lines represent IQR of conventional Swiss Webster mice and the red *X* indicates the microbiota density of the original source fecal sample.

Figure S5

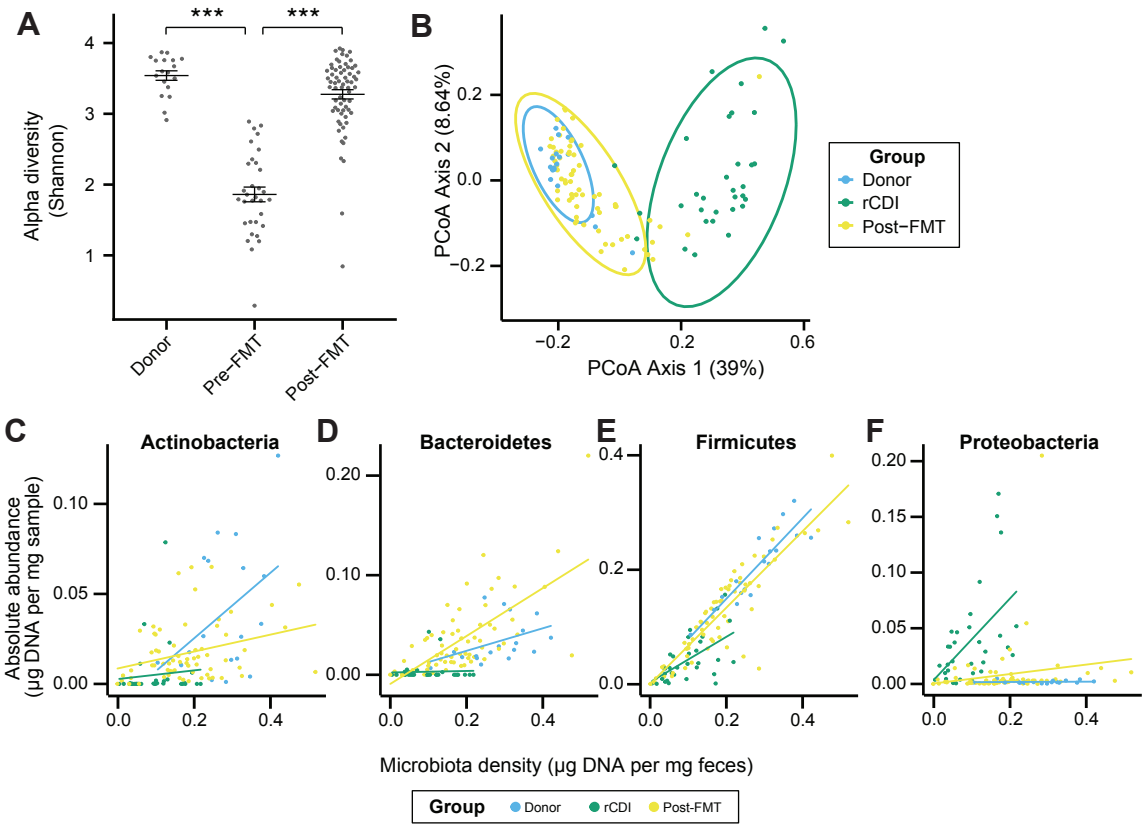

Figure S5. Related to Figure 5. FMT changes the microbiome of individuals with rCDI to resemble that of healthy donors.

(**A**) Alpha diversity in rCDI is significantly lower than in healthy individuals used as FMT donors. This change in alpha diversity is restored by FMT.

(**B**) Principal coordinates analysis of unifrac distances based on the absolute abundances of OTUs in healthy FMT donors and rCDI before and after FMT.

(**C-F**) The rCDI microbiota density is driven largely by the abundance of Proteobacteria and Firmicutes. In healthy donors and individuals following FMT, Proteobacteria are present at a constant absolute abundance, and microbiota density is driven by Firmicutes, Bacteroidetes, and Actinobacteria. Points represent individual subjects and colors indicate their health status In **A**, bars indicate mean ± SEM. ***$p < 0.001$. In **B**, points represent individual samples. Ellipses indicate the 95% confidence interval of distribution of points.

Supplemental tables

Table S1. Related to Figure 1. Mammalian sample information.

Table S2. Related to Figures 3 and 4, and Methods. Antibiotics used in mouse experiments.

Table S3. Related to Figure 3. Transcript expression correlated with microbiota density.

References

Atarashi, K., Tanoue, T., Shima, T., Imaoka, A., Kuwahara, T., Momose, Y., Cheng, G., Yamasaki, S., Saito, T., Ohba, Y., et al. (2011). Induction of colonic regulatory T cells by indigenous Clostridium species. Science (New York, N.Y.) *331*, 337–341.

Bäckhed, F., Ding, H., Wang, T., Hooper, L.V., Koh, G.Y., Nagy, A., Semenkovich, C.F., and Gordon, J.I. (2004). The gut microbiota as an environmental factor that regulates fat storage. Proceedings of the National Academy of Sciences of the United States of America *101*, 15718–15723.

Blaser, M.J. (2014). Missing microbes : how the overuse of antibiotics is fueling our modern plagues.

Bongers, G., Pacer, M.E., Geraldino, T.H., Chen, L., He, Z., Hashimoto, D., Furtado, G.C., Ochando, J., Kelley, K.A., Clemente, J.C., et al. (2014). Interplay of host microbiota, genetic perturbations, and inflammation promotes local development of intestinal neoplasms in mice. The Journal of Experimental Medicine *211*, 457–472.

Britton, G.J., Contijoch, E.J., Mogno, I., Vennaro, O.H., Llewellyn, S.R., Ng, R., Li, Z., Mortha, A., Merad, M., Das, A., et al. (2018). Inflammatory bowel disease microbiotas alter gut CD4 T-cell homeostasis and drive colitis in mice. BioRxiv 276774.

Bryant, H.U., Kuta, C.C., Story, J.A., and Yim, G.K. (1988). Stress- and morphine-induced elevations of plasma and tissue cholesterol in mice: reversal by naltrexone. Biochemical Pharmacology *37*, 3777–3780.

Caporaso, J.G., Kuczynski, J., Stombaugh, J., Bittinger, K., Bushman, F.D., Costello, E.K., Fierer, N., Peña, A.G., Goodrich, J.K., Gordon, J.I., et al. (2010). QIIME allows analysis of high-throughput community sequencing data. Nature Methods *7*, 335–336.

DeSantis, T.Z., Hugenholtz, P., Larsen, N., Rojas, M., Brodie, E.L., Keller, K., Huber, T., Dalevi, D., Hu, P., and Andersen, G.L. (2006). Greengenes, a Chimera-Checked 16S rRNA Gene Database and Workbench Compatible with ARB. Applied and Environmental Microbiology *72*, 5069–5072.

Dethlefsen, L., and Relman, D.A. (2011). Incomplete recovery and individualized responses of the human distal gut microbiota to repeated antibiotic perturbation. Proceedings of the National Academy of Sciences of the United States of America *108 Suppl*, 4554–4561.

Dethlefsen, L., Huse, S., Sogin, M.L., and Relman, D.A. (2008). The pervasive effects of an antibiotic on the human gut microbiota, as revealed by deep 16S rRNA sequencing. PLoS Biology *6*, e280.

Edgar, R., Domrachev, M., and Lash, A.E. (2002). Gene Expression Omnibus: NCBI gene expression and hybridization array data repository. Nucleic Acids Research *30*, 207–210.

Faith, J.J., McNulty, N.P., Rey, F.E., and Gordon, J.I. (2011). Predicting a human gut microbiota's response to diet in gnotobiotic mice. Science (New York, N.Y.) *333*, 101–104.

Faith, J.J., Guruge, J.L., Charbonneau, M., Subramanian, S., Seedorf, H., Goodman, A.L., Clemente, J.C., Knight, R., Heath, A.C., Leibel, R.L., et al. (2013). The long-term stability of the human gut microbiota. Science (New York, N.Y.) *341*, 1237439.

Faith, J.J., Ahern, P.P., Ridaura, V.K., Cheng, J., and Gordon, J.I. (2014). Identifying Gut Microbe-Host Phenotype Relationships Using Combinatorial Communities in Gnotobiotic Mice. Science Translational Medicine *6*, 220ra11–220ra11.

Frank, D.N., St. Amand, A.L., Feldman, R.A., Boedeker, E.C., Harpaz, N., and Pace, N.R. (2007). Molecular-phylogenetic characterization of microbial community imbalances in human inflammatory bowel diseases. Proceedings of the National Academy of Sciences *104*, 13780–13785.

Frazee, A.C., Pertea, G., Jaffe, A.E., Langmead, B., Salzberg, S.L., and Leek, J.T. (2015). Ballgown bridges the gap

between transcriptome assembly and expression analysis. Nature Biotechnology *33*, 243–246.

Geuking, M.B., Cahenzli, J., Lawson, M.A., Ng, D.C., Slack, E., Hapfelmeier, S., McCoy, K.D., and Macpherson, A.J. (2011). Intestinal Bacterial Colonization Induces Mutualistic Regulatory T Cell Responses. Immunity *34*, 794–806.

Gevers, D., Kugathasan, S., Denson, L.A., Vázquez-Baeza, Y., Van Treuren, W., Ren, B., Schwager, E., Knights, D., Song, S.J., Yassour, M., et al. (2014). The treatment-naive microbiome in new-onset Crohn's disease. Cell Host & Microbe *15*, 382–392.

Gophna, U., Sommerfeld, K., Gophna, S., Doolittle, W.F., and Veldhuyzen Van Zanten, S.J. (2006). Differences between tissue-associated intestinal microfloras of patients with Crohn's disease and ulcerative colitis. Journal of Clinical Microbiology *44*, 4136–4141.

Hinnant, R.T., and Kothmann, M.M. (1988). Collecting, drying, and preserving feces for chemical and microhistological analysis. Journal of Range Management *41*, 168–171.

Hirten, R.P., Grinspan, A., Fu, S.-C., Luo, Y., Suarez-Farinas, M., Rowland, J., Contijoch, E.J., Mogno, I., Yang, N., Luong, T., et al. (2018). Microbial Engraftment and Efficacy of Fecal Microbiota Transplant for Clostridium difficile Patients With and Without IBD. BioRxiv 267492.

Hothorn, T., Bretz, F., and Westfall, P. (2008). Simultaneous Inference in General Parametric Models. Biometrical Journal *50*, 346–363.

Ivanov, I.I., Atarashi, K., Manel, N., Brodie, E.L., Shima, T., Karaoz, U., Wei, D., Goldfarb, K.C., Santee, C.A., Lynch, S.V., et al. (2009). Induction of Intestinal Th17 Cells by Segmented Filamentous Bacteria. Cell *139*, 485–498.

Jacobs, J.P., Goudarzi, M., Singh, N., Tong, M., McHardy, I.H., Ruegger, P., Asadourian, M., Moon, B.-H., Ayson, A., Borneman, J., et al. (2016). A Disease-Associated Microbial and Metabolomics State in Relatives of Pediatric Inflammatory Bowel Disease Patients. Cellular and Molecular Gastroenterology and Hepatology *2*, 750–766.

Kashyap, P.C., Marcobal, A., Ursell, L.K., Larauche, M., Duboc, H., Earle, K.A., Sonnenburg, E.D., Ferreyra, J.A., Higginbottom, S.K., Million, M., et al. (2013). Complex interactions among diet, gastrointestinal transit, and gut microbiota in humanized mice. Gastroenterology *144*, 967–977.

Kim, D., Langmead, B., and Salzberg, S.L. (2015). HISAT: a fast spliced aligner with low memory requirements. Nature Methods *12*, 357–360.

Larsson, H., Carlsson, E., Junggren, U., Olbe, L., Sjöstrand, S.E., Skånberg, I., and Sundell, G. (1983). Inhibition of gastric acid secretion by omeprazole in the dog and rat. Gastroenterology *85*, 900–907.

Llewellyn, S.R., Britton, G.J., Contijoch, E.J., Vennaro, O.H., Mortha, A., Colombel, J.-F., Grinspan, A., Clemente, J.C., Merad, M., and Faith, J.J. (2017). Interactions between diet and the intestinal microbiota alter intestinal permeability and colitis severity in mice. Gastroenterology *0*.

Magoč, T., and Salzberg, S.L. (2011). FLASH: fast length adjustment of short reads to improve genome assemblies. Bioinformatics (Oxford, England) *27*, 2957–2963.

Mahowald, M.A., Rey, F.E., Seedorf, H., Turnbaugh, P.J., Fulton, R.S., Wollam, A., Shah, N., Wang, C., Magrini, V., Wilson, R.K., et al. (2009). Characterizing a model human gut microbiota composed of members of its two dominant bacterial phyla. Proc Natl Acad Sci U S A *106*, 5859–5864.

McDonald, D., Price, M.N., Goodrich, J., Nawrocki, E.P., DeSantis, T.Z., Probst, A., Andersen, G.L., Knight, R., and Hugenholtz, P. (2012). An improved Greengenes taxonomy with explicit ranks for ecological and evolutionary analyses of bacteria and archaea. The ISME Journal *6*, 610–618.

McMurdie, P.J., and Holmes, S. (2013). phyloseq: an R package for reproducible interactive analysis and graphics of

microbiome census data. PloS One *8*, e61217.

Mortha, A., Chudnovskiy, A., Hashimoto, D., Bogunovic, M., Spencer, S.P., Belkaid, Y., and Merad, M. (2014). Microbiota-Dependent Crosstalk Between Macrophages and ILC3 Promotes Intestinal Homeostasis. Science *343*, 1249288–1249288.

Muller, P.A., Koscsó, B., Rajani, G.M., Stevanovic, K., Berres, M.-L., Hashimoto, D., Mortha, A., Leboeuf, M., Li, X.-M., Mucida, D., et al. (2014). Crosstalk between muscularis macrophages and enteric neurons regulates gastrointestinal motility. Cell *158*, 300–313.

Nitsche, A., Becker, M., Junghahn, I., Aumann, J., Landt, O., Fichtner, I., Wittig, B., and Siegert, W. (2001). Quantification of human cells in NOD/SCID mice by duplex real-time polymerase-chain reaction. Haematologica *86*.

Pertea, M., Pertea, G.M., Antonescu, C.M., Chang, T.-C., Mendell, J.T., and Salzberg, S.L. (2015). StringTie enables improved reconstruction of a transcriptome from RNA-seq reads. Nature Biotechnology *33*, 290–295.

Pertea, M., Kim, D., Pertea, G.M., Leek, J.T., and Salzberg, S.L. (2016). Transcript-level expression analysis of RNA-seq experiments with HISAT, StringTie and Ballgown. Nature Protocols *11*.

Props, R., Kerckhof, F.-M., Rubbens, P., De Vrieze, J., Hernandez Sanabria, E., Waegeman, W., Monsieurs, P., Hammes, F., and Boon, N. (2017). Absolute quantification of microbial taxon abundances. The ISME Journal *11*, 584–587.

R Core Team (2017). R: A language and environment for statistical computing (Vienna, Austria: R Foundation for Statistical Computing).

Relman, D.A., Schmidt, T.M., MacDermott, R.P., and Falkow, S. (1992). Identification of the Uncultured Bacillus of Whipple's Disease. New England Journal of Medicine *327*, 293–301.

Rey, F.E., Gonzalez, M.D., Cheng, J., Wu, M., Ahern, P.P., and Gordon, J.I. (2013). Metabolic niche of a prominent sulfate-reducing human gut bacterium. Proceedings of the National Academy of Sciences of the United States of America *110*, 13582–13587.

Reyes, A., Wu, M., McNulty, N.P., Rohwer, F.L., and Gordon, J.I. (2013). Gnotobiotic mouse model of phage-bacterial host dynamics in the human gut. Proceedings of the National Academy of Sciences of the United States of America *110*, 20236–20241.

Ridaura, V.K., Faith, J.J., Rey, F.E., Cheng, J., Duncan, A.E., Kau, A.L., Griffin, N.W., Lombard, V., Henrissat, B., Bain, J.R., et al. (2013). Gut microbiota from twins discordant for obesity modulate metabolism in mice. Science (New York, N.Y.) *341*, 1241214.

Satinsky, B.M., Gifford, S.M., Crump, B.C., and Moran, M.A. (2013). Use of Internal Standards for Quantitative Metatranscriptome and Metagenome Analysis. Methods in Enzymology *531*, 237–250.

Schloss, P.D., Westcott, S.L., Ryabin, T., Hall, J.R., Hartmann, M., Hollister, E.B., Lesniewski, R.A., Oakley, B.B., Parks, D.H., Robinson, C.J., et al. (2009). Introducing mothur: Open-Source, Platform-Independent, Community-Supported Software for Describing and Comparing Microbial Communities. Applied and Environmental Microbiology *75*, 7537–7541.

Seekatz, A.M., Aas, J., Gessert, C.E., Rubin, T.A., Saman, D.M., Bakken, J.S., and Young, V.B. (2014). Recovery of the gut microbiome following fecal microbiota transplantation. MBio *5*, e00893–14.

Segata, N., Waldron, L., Ballarini, A., Narasimhan, V., Jousson, O., and Huttenhower, C. (2012). Metagenomic microbial community profiling using unique clade-specific marker genes. Nature Methods *9*, 811–814.

Shankar, V., Hamilton, M.J., Khoruts, A., Kilburn, A., Unno, T., Paliy, O., and Sadowsky, M.J. (2014). Species and genus level resolution analysis of gut microbiota in Clostridium difficile patients following fecal microbiota transplantation. Microbiome *2*, 13.

Sievers, F., Wilm, A., Dineen, D., Gibson, T.J., Karplus, K., Li, W., Lopez, R., McWilliam, H., Remmert, M., Söding, J., et

al. (2011). Fast, scalable generation of high-quality protein multiple sequence alignments using Clustal Omega. Molecular Systems Biology *7*, 539.

Sonnenburg, E.D., Smits, S.A., Tikhonov, M., Higginbottom, S.K., Wingreen, N.S., and Sonnenburg, J.L. (2016). Diet-induced extinctions in the gut microbiota compound over generations. Nature *529*, 212–215.

Stämmler, F., Gläsner, J., Hiergeist, A., Holler, E., Weber, D., Oefner, P.J., Gessner, A., and Spang, R. (2016). Adjusting microbiome profiles for differences in microbial load by spike-in bacteria. Microbiome *4*, 28.

Vaishnava, S., Yamamoto, M., Severson, K.M., Ruhn, K. a, Yu, X., Koren, O., Ley, R., Wakeland, E.K., and Hooper, L.V. (2011). The Antibacterial Lectin RegIII Promotes the Spatial Segregation of Microbiota and Host in the Intestine. Science *334*, 255–258.

Vandeputte, D., Kathagen, G., D'hoe, K., Vieira-Silva, S., Valles-Colomer, M., Sabino, J., Wang, J., Tito, R.Y., De Commer, L., Darzi, Y., et al. (2017). Quantitative microbiome profiling links gut community variation to microbial load. Nature *551*, 507.

Wostmann B, and Bruckner-Kardoss, E. (1959). Development of cecal distention in germ-free baby rats. The American Journal of Physiology *197*, 1345–1346.

Zhang, D., Chen, G., Manwani, D., Mortha, A., Xu, C., Faith, J.J., Burk, R.D., Kunisaki, Y., Jang, J.-E., Scheiermann, C., et al. (2015). Neutrophil ageing is regulated by the microbiome. Nature *525*, 528–532.